Mutational Analysis of the SARS Virus Nsp15 Endoribonuclease: Identification of Residues Affecting Hexamer Formation

Linda A. Guarino[1,2,3]*, Kanchan Bhardwaj[1], Wen Dong[3], Jingchuan Sun[2] Andreas Holzenburg[1,2,4] and Cheng Kao[1]

[1]*Department of Biochemistry and Biophysics, Texas A&M University, College Station Texas 77843-2128, USA*

[2]*Department of Biology, Texas A&M University, College Station, Texas 77843-2128 USA*

[3]*Department of Entomology Texas A&M University, College Station, Texas 77843-2128 USA*

[4]*Department of Microscopy and Imaging Center, Texas A&M University, College Station Texas 77843-2128, USA*

The severe acute respiratory syndrome (SARS) coronavirus virus non-structural protein 15 is a Mn^{2+}-dependent endoribonuclease with specificity for cleavage at uridylate residues. To better understand structural and functional characteristics of Nsp15, 22 mutant versions of Nsp15 were produced in *Escherichia coli* as His-tagged proteins and purified by metal-affinity and ion-exchange chromatography. Nineteen of the mutants were soluble and were analyzed for enzymatic activity. Six mutants, including four at the putative active site, were significantly reduced in endoribonuclease activity. Two of the inactive mutants had unusual secondary structures compared to the wild-type protein, as measured by circular dichroism spectroscopy. Gel-filtration analysis, velocity sedimentation ultracentrifugation, and native gradient pore electrophoresis all showed that the wild-type protein exists in an equilibrium between hexamers and monomers in solution, with hexamers dominating at micromolar protein concentration, while native gradient pore electrophoresis also revealed the presence of trimers. A mutant in the N terminus of Nsp15 was impaired in hexamer formation and had low endoribonuclease activity, suggesting that oligomerization is required for endoribonuclease activity. This idea was supported by titration experiments showing that enzyme activity was strongly concentration-dependent, indicating that oligomeric Nsp15 is the active form. Three-dimensional reconstruction of negatively stained single particles of Nsp15 viewed by transmission electron microscopic analysis suggested that the six subunits were arranged as a dimer of trimers with a number of cavities or channels that may constitute RNA binding sites.

© 2005 Elsevier Ltd. All rights reserved.

Keywords: nidovirus; RNA processing; viral replication; single molecule microscopy

*Corresponding author

Introduction

Severe acute respiratory syndrome (SARS) emerged in Guangdong Province, China in 2002 and eventually spread to 30 countries. More than 8400 cases and approximately 920 deaths were confirmed as SARS-related†. SARS is caused by a coronavirus (SARS-CoV), which has a positive-strand RNA genome of approximately 30 kb in length with a 5′ cap and 3′ poly(A) tail.[1,2] Coronaviruses have been subdivided into three phylogenetic groups. Groups 1 and 2 infect mammals, usually resulting in only a mild respiratory distress. Group 3 infects birds and includes the causative agent of a severe disease that is economically significant for the poultry industry.[3,4] Analysis of the complete genomes of over a dozen SARS-CoV isolates from around the world indicate that SARS-CoV is not a mutant or a recombinant of known coronaviruses, but a novel one that acquired the ability to infect humans.[5] Isolation of a nearly identical coronavirus from civet cats, raccoon dogs, and badgers, suggests SARS-CoV jumped species from its natural animal host to humans.[6]

Abbreviations used: SARS, severe acute respiratory syndrome; CoV, coronavirus; Nsp, non-structural protein; XendoU, *Xenopus* endonuclease U.

E-mail address of the corresponding author: lguarino@tamu.edu

† http://www.cdc.gov/ncidod/sars/faq.htm

Coronaviruses produce two large polyproteins that are proteolytically processed to yield replication-associated proteins named Nsp1-16, and several structural proteins that are translated from sub-genomic RNAs. The sub-genomic RNAs have a common 5′ leader sequence that is derived from the 5′ end of genomic RNA. One current model predicts that fusion of the leader to the sub-genomic RNA occurs during minus-strand RNA synthesis, when the replicase ternary complex translocates at specific positions in the template RNA and then resumes RNA synthesis near the 5′ end.[7–9] Alternatively, a leader-prime mechanism for plus-strand synthesis has been proposed.[3,10] This model states that a free 5′ leader anneals to a complementary sequence at one of the intergenic sites and primes transcription of a sub-genomic RNA.

Given the large genomes of coronaviruses and a need for discontinuous transcription to generate sub-genomic transcripts, they are expected to encode novel RNA processing functions. Indeed, three such proteins have been identified by sequence homology: Nsp14, a putative exonuclease; Nsp15, an endoribonuclease; and Nsp16, a putative RNA methyltransferase.[11,12] Recently, we confirmed the predicted function for SARS-CoV Nsp15, and showed that its activity was enhanced by Mn^{2+} and that cleavage was specific for uridylate residues.[13] Similar results were reported by Ivanov et al.,[14] who also demonstrated that the Nsp15 ortholog of human coronavirus was essential for virus replication. RNA endoribonuclease activity is unusual among plus-strand RNA viruses, suggesting that it could be a target for antiviral development. In addition, the high specificity for unpaired uridylate residues suggests that Nsp15 could be used to study RNA structure and function.

To better understand structure and function aspects of Nsp15, we undertook a mutational screen to identify essential residues. Several mutants were identified with impaired function. These mutants and wild-type proteins were screened for the ability to form higher-order structures and a mutant deficient in hexamer formation as well as a mutant locked into a hexamer state were identified.

Results

Structure–function analysis of Nsp15

Previously, we showed that Nsp15 expressed in *Escherichia coli* was a uridine-specific endonuclease.[13] To define the amino acid residues that are required for activity, we constructed 20 single and two double mutant versions of Nsp15 (Figure 1). Three residues (H234, H249 and K289) selected for mutagenesis were previously noted due to their conservation among coronaviruses and members of the *Xenopus* endonuclease U (XendoU) family of uridine-specific endoribonucleases.[11] The remaining residues targeted for mutagenesis were all aspartate or glutamate, and are highly conserved
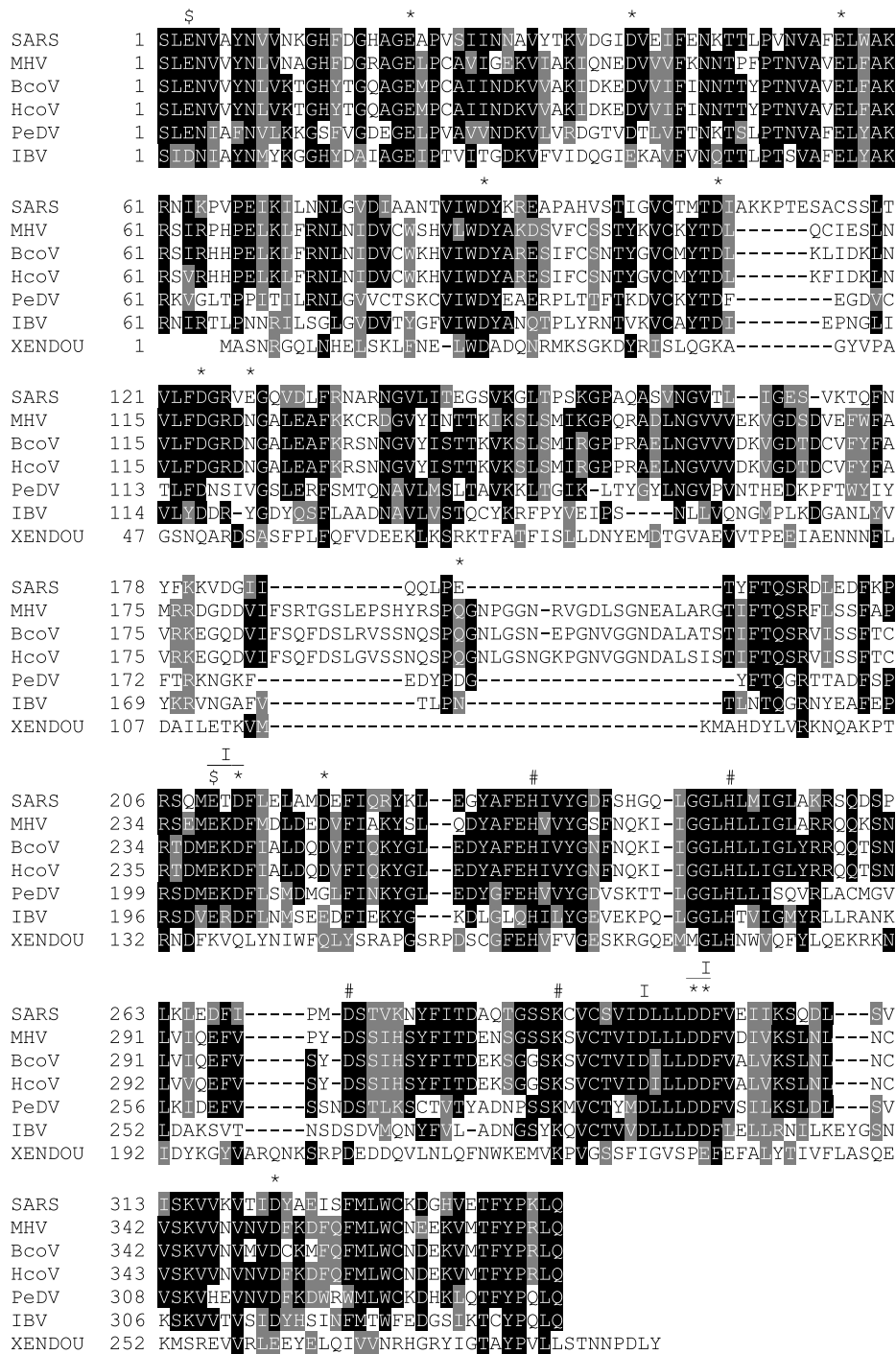
among coronaviruses and, in some cases, conserved in XendoU.

Wild-type and alanine-substituted versions of Nsp15 were produced as His-tagged proteins and purified by metal affinity and ion-exchange chromatography. SDS-PAGE showed that most of mutant proteins were purified to single-band homogeneity (Figure 2(a)). Some preparations contained a band migrating at the position of a dimer even in denaturing SDS-PAGE (most obvious for D272A), but other contaminants were not evident. Three mutant constructs, the single substitution D296A and two double substitutions E210A/D212A and D300A/D301A, produced insoluble protein and were not characterized further.

Endonuclease activity was assayed using an RNA substrate corresponding to the SARS-CoV TRS sequence for the Spike protein sub-genomic RNA. The advantage of this RNA over those used in our previous experiments[13] is that it contains a single uridine residue, and so produces a single radio-labeled product that can be quantified easily. All mutants were tested at 62.5 nM, under conditions in which the wild-type enzyme exhausted approximately 40% of the substrate (Figure 2(a) and Supplementary Data Figure 1). Most of the mutants showed a level of activity that was within twofold of the wild-type enzyme, indicating that their activities were not affected significantly by the substitution.

To focus attention on residues most likely to be significant, only mutants with less than 20% of the wild-type level of activity were selected for further analysis. These six mutants were tested at a higher range of concentrations. Four mutants showed no activity, even when added at concentrations up to 200-fold higher than wild-type (Figure 2(b)). These substituted residues, H234A, H249A, D272A, and K289A, are highly conserved among coronavirus orthologs, as well as in all members of the XendoU family, suggesting that they are directly involved in catalysis. It may also be significant that yields of three of these inactive proteins (H234A, H249A, and K289A) were approximately 1000-fold higher than wild-type protein (data not shown), suggesting that they were less toxic to bacteria. D272A was synthesized at levels equivalent to the histidine and lysine mutants, but was mostly insoluble. Thus, the final yield of D272A was low, but the high level of synthesis suggested that it was also not toxic to cells due to its complete lack of activity. Bacteria harboring these four expression plasmids also grew faster than those with wild-type plasmid or the other substitutions, suggesting that even a low-level expression of active protein was detrimental to the cells. Mutants E3A and E210A showed measurable activity, but were significantly reduced compared to wild-type.

In considering possible mechanisms of action for Nsp15, the collection of mutants could represent proteins that are impaired for different activities of the protein. For example, some mutants may fail to bind Mn^{2+}, some may be impaired in substrate binding, while others could map to residues that

```
                $                    *                   *                   *
SARS     1   SLENVAYNVVNKGHFDGHAGEAPVSIINNAVYTKVDGIDVEIFENKTTLPVNVAFELWAK
MHV      1   SLENVVYNLVNAGHFDGRAGELPCAVIGEKVIAKIQNEDVVVFKNNTPFPTNVAVELFAK
BcoV     1   SLENVVYNLVKTGHYTGQAGEMPCAIINDKVVAKIDKEDVVIFINNTTYPTNVAVELFAK
HcoV     1   SLENVVYNLVKTGHYTGQAGEMPCAIINDKVVAKIDKEDVVIFINNTTYPTNVAVELFAK
PeDV     1   SLENIAFNVLKKGSFVGDEGELPVAVVNDKVLVRDGTVDTLVFTNKTSLPTNVAFELYAK
IBV      1   SIDNIAYNMYKGGHYDAIAGEIPTVITGDKVFVIDQGIEKAVFVNQTTLPTSVAFELYAK

                                         *                   *
SARS    61   RNIKPVPEIKILNNLGVDIAANTVIWDYKREAPAHVSTIGVCTMTDIAKKPTESACSSLT
MHV     61   RSIRPHPELKLFRNLNIDVCWSHVLWDYAKDSVFCSSTYKVCKYTDL------QCIESLN
BcoV    61   RSIRHHPELKLFRNLNIDVCKHVIWDYARESIFCSNTYGVCMYTDL------KLIDKLN
HcoV    61   RSVRHHPELKLFRNLNIDVCWKHVIWDYARESIFCSNTYGVCMYTDI------KFIDKLN
PeDV    61   RKVGLTPPITILRNLGVVCTSKCVIWDYEAFRPLTTFTKDVCKYTDF--------EGDVC
IBV     61   RNIRTLPNNRILSGLGVDVTYGFVIWDYANQTPLYRNTVKVCAYTDI-------EPNGLI
XENDOU   1     MASNRGQLNHELSKLFNE-LWDADQNRMKSGKDYRISLQGKA--------GYVPA

                    *   *
SARS   121   VLFDGRVEGQVDLFRNARNGVLITEGSVKGLTPSKGPAQASVNGVTL--IGES-VKTQFN
MHV    115   VLFDGRDNGALEAFKKCRDGVYINTTKIKSLSMIKGPQRADLNGVVVEKVGDSDVEFWFA
BcoV   115   VLFDGRDNGALEAFKRSNNGVYISTTKVKSLSMIRGPPRAELNGVVVDKVGDTDCVFYFA
HcoV   115   VLFDGRDNGALEAFKRSNNGVYISTTKVKSLSMIRGPPRAELNGVVVDKVGDTDCVFYFA
PeDV   113   TLFDNSIVGSLERFSMTQNAVLMSLTAVKKLTGIK-LTYGYLNGVPVNTHEDKPFTWYIY
IBV    114   VLYDDR-YGDYQSFLAADNAVLVSTQCYKRFPYVEIPS----NLLVQNGMPLKDGANLYV
XENDOU  47   GSNQARDSASFPLFQFVDEEKLKSRKTFAIFISLLDNYEMDTGVAEVVTPEEIAENNNFL

                                *
SARS   178   YFKKVDGII-----------QQLPE--------------------TYFTQSRDLEDFKP
MHV    175   MRRDGDDVIFSRTGSLEPSHYRSPQGNPGGN-RVGDLSGNEALARGTIFTQSRFLSSFAP
BcoV   175   VRKEGQDVIFSQFDSLRVSSNQSPQGNLGSN-EPGNVGGNDALATSTIFTQSRVISSFTC
HcoV   175   VRKEGQDVIFSQFDSLGVSSNQSPQGNLGSNGKPGNVGGNDALSISTIFTQSRVISSFTC
PeDV   172   FTRKNGKF-----------EDYPDG---------------------YFTQGRTTADFSP
IBV    169   YKRVNGAFV-----------TLPN--------------------TLNTQGRNYEAFEP
XENDOU 107   DAILETKVM-----------------------------------KMAHDYLVRKNQAKPT

                    I
                    $ *     *               #               #
SARS   206   RSQMETDFLELAMDEFIQRYKL--EGYAFEHIVYGDFSHGQ-IGGLHLMIGIAKRSQDSP
MHV    234   RSEMEKDFMDLDEDVFIAKYSL--QDYAFEHVVYGSFNQKI-IGGLHLLIGIARRQQKSN
BcoV   234   RTDMEKDFIALDQDVFIQKYGL--EDYAFEHIVYGDFNQKI-IGGLHLLIGLYRRQQTSN
HcoV   235   RTDMEKDFIALDQDVFIQKYGL--EDYAFEHIVYGNFNQKI-IGGLHLLIGLYRRQQTSN
PeDV   199   RSDMEKDFISMDMGLFINKYGI--EDYGFEHVVYGDVSKTT-LGGLHLLISQVRLACMGV
IBV    196   RSDVERDFINMSEEDFIEKYG---KDLGLQHILYGEVEKPQ-IGGLHTVIGMYRLLRANK
XENDOU 132   RNDFKVQLYNIWFQLYSRAPGSRPDSCGFEHVFVGESKRGQEMMGLHNWVQFYLQEKRKN

                #                   #           I
                                                **
SARS   263   LKLEDFI-----PM-DSTVKNYFITDAQTGSSKCVCSVIDLLLDDFVEIIKSQDI---SV
MHV    291   LVIQEFV-----PY-DSSIHSYFITDENSGSSKSVCTVIDLLLDDFVDIVKSLNI---NC
BcoV   291   LVIQEFV-----SY-DSSIHSYFITDEKSGGSKSVCTVIDILLLDDFVALVKSLNI---NC
HcoV   292   LVVQEFV-----SY-DSSIHSYFITDEKSGGSKSVCTVIDILLLDDFVALVKSLNI---NC
PeDV   256   LKIDEFV-----SSNDSTLKSCTVTYADNPSSKMVCTYMDLLLDDFVSILKSLDI---SV
IBV    252   LDAKSVT-----NSDSDVMQNYFVL-ADNGSYKQVCTVVDLLLDDFLELLRNILKEYGSN
XENDOU 192   IDYKGYVARQNKSRPDEDDQVLNLQFNWKEMVKPVGSSFIGVSPEFEFALYTIVFLASQE

                    *
SARS   313   ISKVVKVTIDYAEISFMLWCKDGHVETFYPKLQ
MHV    342   VSKVVNVNVDFKDFQFMLWCNEEKVMTFYPRLQ
BcoV   342   VSKVVNVMVDCKMFQFMLWCNDEKVMTFYPRLQ
HcoV   343   VSKVVNVNVDFKDFQFMLWCNDEKVMTFYPRLQ
PeDV   308   VSKVHEVNVDFKDWRWMLWCKDHKLQTFYPQLQ
IBV    306   KSKVVTVSIDYHSINFMTWFEDGSIKTCYPQLQ
XENDOU 252   KMSREVVRLEEYELQIVVNRHGRYIGTAYPVLLSTNNPDLY
```
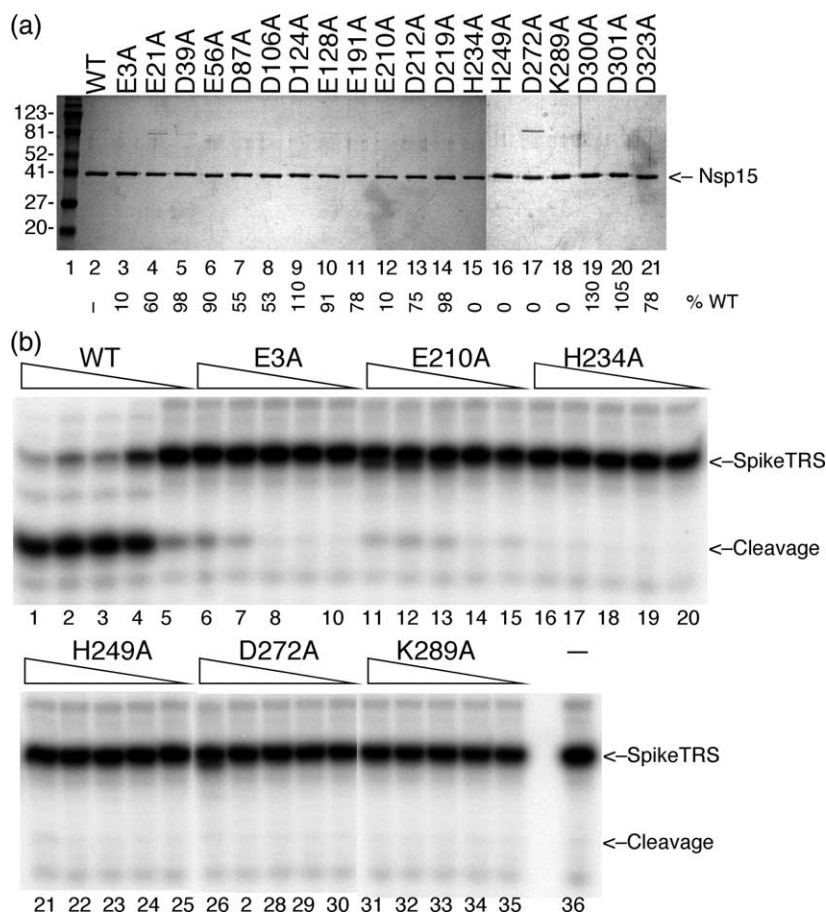
Figure 1. Alignments of the Nsp15 orthologs from several coronaviruses and *X. laevis* EndoU. The amino acid sequence of the SARS Nsp15 was aligned with orthologs of murine hepatitis virus (MHV; AAF19384), bovine coronavirus (BCoV; AAL57305), human coronavirus (HCoV; YP173236), porcine endemic diarrhea virus (PeDV; AAK38661), infectious bronchitis virus (IBV; AAT70770), and *Xenopus laevis* endoU (XendoU; CAD45344) using PSI-BLAST[32] and shaded using the BoxShade server. Gaps in the sequence alignment are denoted by hyphens. Residues that are identical in at least four of the seven sequences are shown in bold. Conserved amino acid residues are shaded. The symbols above the sequence denote residues that were mutated to alanine: *, active (within 50% wild-type level); $, impaired (less than 10% wild-type activity); #, inactive; I, insoluble.

play direct roles in the catalysis of phosphodiester bond hydrolysis. We also considered the possibility that mutation of surface charged groups could affect protein–protein interactions of Nsp15 with itself, which is the focus of this work.

Nsp15 oligomerization

Gel-filtration chromatography was used to examine the native molecular mass of Nsp15. When the wild-type protein was filtered through a

(a)

<- Nsp15

1 2 3 4 5 6 7 8 9 10 11 12 13 14 15 16 17 18 19 20 21

– 10 60 98 90 55 53 110 91 78 10 75 98 0 0   0 0 130 105 78   % WT

(b)

Figure 2. Purification and activity of mutant versions of Nsp15. (a) SDS-PAGE analysis of Nsp15 mutant proteins purified from *E. coli*. Protein (1 μg per lane) purified by Mono Q chromatography was analyzed on SDS/10% polyacrylamide gels. The migration of pre-stained molecular mass markers (lane 1) is indicated on the left. The identity of each mutant is indicated above each lane (lanes 2–21). A summary of the activity of each mutant protein is shown below the lane numbers. Activities are expressed as a percentage of wild-type activity. (b) Titrations of impaired versions of Nsp15. SpikeTRS (5 μM) was incubated with different concentrations of wild-type (WT) Nsp15 or the indicated mutant protein (1200, 600, 300, 150, 75 nM). After 30 min at 30 °C, reactions were stopped by the addition of formamide dye and electrophoresed through a 3 M urea, 28% polyacrylamide gel. The amount of cleavage product was quantified by PhosphorImager analysis.

Superdex 200 size-exclusion column at an initial concentration of 5 μM, two distinct UV-absorbing peaks were observed (Figure 3). Comparison of the elution volumes relative to marker proteins filtered through the same column indicated a molecular mass of 47,900 Da for the smaller peak eluting at 15.08 ml. This peak presumably represents monomeric Nsp15, since the expected molecular mass for the His-tagged protein was 40,790 Da. The calculated mass for the larger peak, eluting at 11.41 ml, was 252,000 Da, which is consistent with formation of hexamers. Quantification of the peak area indicated that 90% of total protein was hexameric.

The elution patterns for mutants E210A, H249A, and D272A were similar to wild-type with approximately 90% of the protein migrating as hexamers (data not shown). As a control, we also analyzed two of the active mutants, E56 and D212, by gel-filtration chromatography. Both of these showed monomer and hexamer peaks in approximately the same proportions as wild-type protein (data not shown). The other three mutants showed patterns that differed from wild-type. In E3A, the relative abundance of monomers and hexamers was shifted toward monomers, with approximately 52% of total protein in the monomeric peak. In addition, there was a shoulder between monomers and hexamers, consistent with an intermediate trimeric form. In K289A, the equilibrium was shifted toward

hexamers, as the monomer peak was only 2% of total protein. In addition, a small peak, corresponding to 3% of total protein, eluted at 9.81 ml, which is the expected position of Nsp15 dodecamers. H234 was more similar to wild-type, except that the proportion of monomers was 34%, significantly higher than observed with wild-type. In addition, a small peak at the position of trimers was seen with H234 (data not shown).

This result was confirmed using sedimentation velocity analytical centrifugation (Figure 4). We also took advantage of the multiple tube rotor to analyze effects of protein concentration simultaneously and the addition of Mn^{2+} on hexamerization. When analyzed at 0.1 μM in the absence of Mn^{2+}, wild-type Nsp15 sedimented as two distinct species of 6.3 S and 1.8 S, which are labeled H and M, respectively, in Figure 4(a). The molecular mass was determined by direct fitting with the Lamm equation, and the derived values were within 8% of that expected for monomers (40.8 kDa) and 1% of the predicted hexamer molecular mass (285 kDa). We previously showed that wild-type Nsp15 underwent a large conformational change when titrated with Mn^{2+}, but not Mg^{2+}, by change in intrinsic fluorescence of Nsp15.[13] Therefore, we tested the addition of 10 mM Mn^{2+} to see if oligomerization was responsible for this shift. We found that Mn^{2+} changed the proportion of hexamers from 63% to
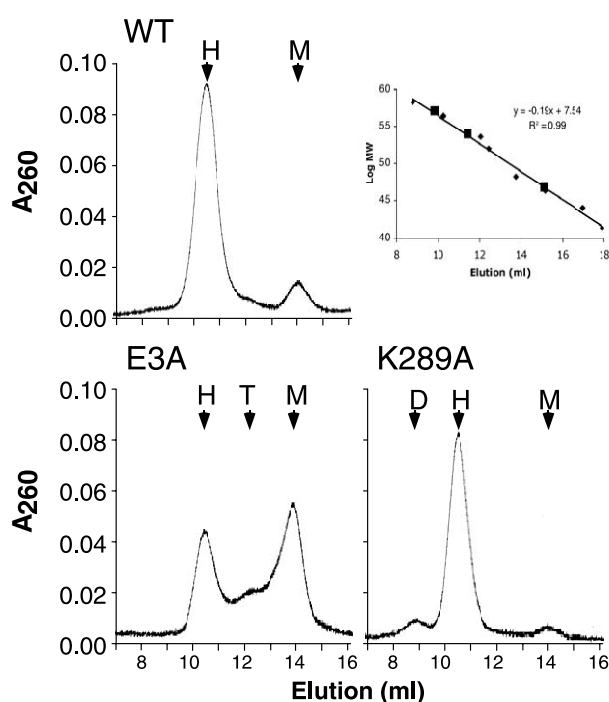
Figure 3. Gel-filtration of Nsp15. Elution profiles for wild-type (WT) Nsp15 and mutant versions E3A and K289A. Molecular masses were calculated relative to native molecular mass markers as shown in the inset. The expected positions for hexamer (H), trimer (T) and monomer (M) are shown in each panel where relevant. The elution profiles for four inactive mutants (E210A, H249A, and D272A) and two mutants with wild-type activity (E56A and D212A) were similar to WT, and were omitted from the Figure for simplicity. Mutant H234A was also similar to WT, although the monomer proportion was higher. The inset shows the standard curve for the protein markers (triangles) and the predicted molecular masses for the different forms of Nsp15 (squares).

66%, indicating that alterations in oligomerization was probably not responsible for the decreased intrinsic fluorescence observed previously. Gel-filtration chromatography performed in the presence of 5 mM Mn^{2+} also caused only a slight shift from monomer to hexamer, confirming that Mn^{2+} has only a minor effect on the oligomerization state (data not shown). When Nsp15 was examined for the ratio of monomers and hexamers at higher protein concentration (1 µM), however, the relative amount of hexamer increased to 85% (Figure 4(b)). These results indicate that protein concentration strongly affected the equilibrium between the monomeric and hexameric states of the protein, while Mn^{2+} primarily affected the local conformation within monomer units.

The monomer–hexamer distribution of the K289A and E3A mutants was also analyzed by analytical ultracentrifugation (Figure 4(c)). The two mutants and wild-type were centrifuged at 1 µM, under conditions where wild-type protein was

about 15% monomeric. The two mutants, however, showed patterns that were significantly different. K289A was primarily hexameric, with only a small peak at the position of monomers, indicating that the equilibrium was shifted toward oligomerization. In contrast, E3A was predominantly in the monomeric state, suggesting that it was defective for hexamer formation at that concentration. These results are in good agreement with those from the gel-filtration analysis (Figure 3)

Gradient pore electrophoresis

Since multiple conditions and single amino acid substitutions could all affect Nsp15 oligomerization, we wanted to compare the state of oligomerization of wild-type and mutant Nsp15 proteins in one assay. Hence, we used electrophoresis on native pore gradient gels (Figure 5(a)). This is an equilibrium system, in which protein migration slows as they move through increasing acrylamide concentration and, eventually, mobility decreases to a minimum at a position that is a direct reflection of its molecular mass. Gels were loaded with 4 µg of each protein at an initial concentration of 5 µM. Comparison of wild-type Nsp15 migration with native molecular mass markers revealed a high molecular mass complex consistent with that of a hexamer. Also evident was a broader band migrating at the expected positions for trimers and a small monomer band.

Most of the mutant proteins also showed bands at the hexamer, trimer and monomer positions, although the relative abundance of the bands differed somewhat among the mutants. The overall patterns were similar to the gel-filtration results, except that, as with wild-type, there was less hexamer and more trimer. E3A was exclusively in trimeric and monomeric forms, with no evidence of hexamers. K289A showed the greatest proportion of hexamers, and a band consistent with a dodecamer was present.

As a control to show that the alterations in hexamer formation were specific for the mutant forms, we also analyzed six mutants with normal activity. The patterns seen with these mutant versions were indistinguishable from wild-type (Figure 5(b)).

Electron microscopic studies of Nsp15 K289

Due to the large size of the hexamers, it should be possible to visualize single Nsp15 particles in the electron microscope. Mutant K289A was chosen for these studies because it was expressed abundantly and appeared to have a tighter subunit association. The electron micrograph in Figure 6(a) shows a homogeneous and monodisperse population of K289A single particles that are well separated. Single-particle analysis revealed a large number of elongated square-shaped projections and a lesser amount of circular projections exhibiting a pronounced central pore (Figure 6(b)). Two thousand
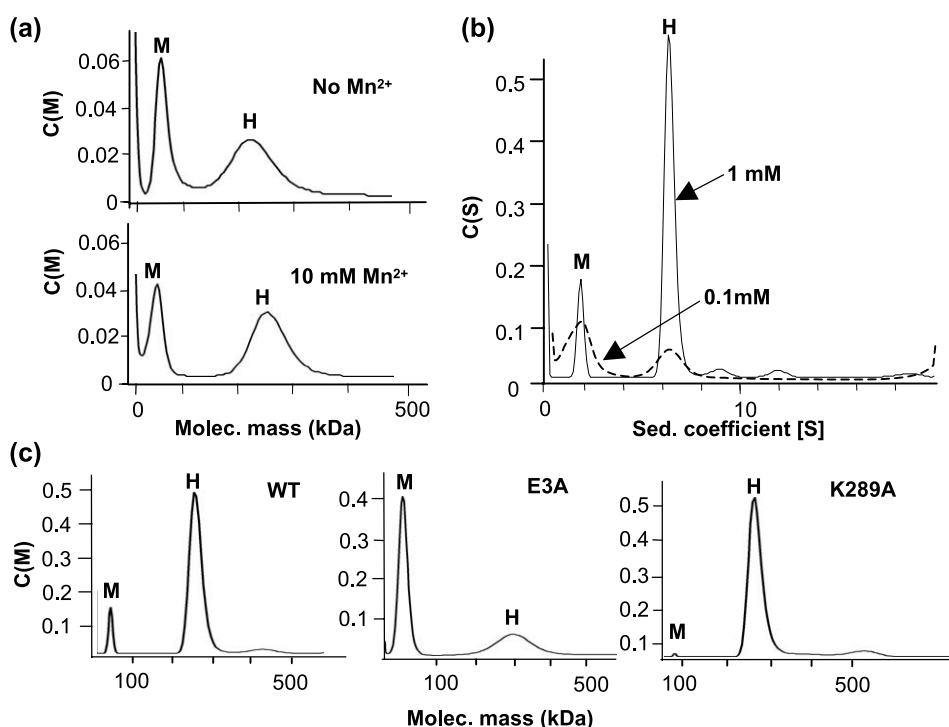
Figure 4. Analysis of factors affecting oligomerization of Nsp15. Sedimentation mass $C(M)$ distributions derived from sedimentation velocity profiles. (a) Sedimentation profiles of wild-type Nsp15 as a function of Mn^{2+} concentration. The data were plotted to show the masses of the samples. (b) $C(S)$ distributions comparing the distribution of the monomer and hexamers as a function of the concentration of wild-type Nsp15. The data were plotted to show the sedimentation coefficients of the samples, with the arrows identifying the profiles from the two concentrations of Nsp15. (c) A comparison of the analytical sedimentation profiles of wild-type and mutant Nsp15 s. All proteins were analyzed at 1 µM concentration and the sedimentation mass ($C(M)$) was derived using SedFit.[26] The identities of the proteins used are indicated at the upper right corner of the panel; monomers (M) and hexamers (H) are identified in each panel.
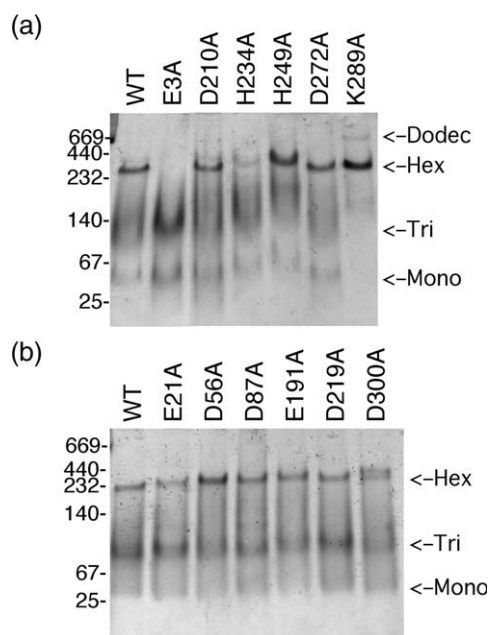
Figure 5. Native gel electrophoresis: 4 µg of each protein was electrophoresed through a 4%–20% polyacrylamide gel, and stained with Coomassie brilliant blue. The predicted migration of hexamers, trimers, and monomers relative to molecular mass markers is shown at the right.

particles were selected and grouped into subclasses as representing various views for 3D reconstruction. During the fifth iterative refinement, the data began to converge and after the eighth refinement cycle, no further improvement was achieved (Figure 7(c)). Although there was a scarcity of face-on projections, as shown by the asymmetric triangle (Figure 6(d)), there was a large number of different side-on views thus permitting a 3D reconstruction (Figure 6(e)). The validation of the reconstruction is, however, critically dependent on choosing the correct point group symmetry. Analysis of the symmetry of the 2D crystals (Figure 7) aided this process greatly. The symmetry of the lattices formed was determined to be consistent with a $p3$ plane group. While the projection map (Figure 7(c)) displays six density maxima per unit cell, the overall distribution of the protein mass followed a triangular arrangement. In addition, there was good agreement between the projection map and the 3D reconstruction when viewed face-on (Figure 6(e)). The large number of side-on views also supported the idea that Nsp15 has a two-layered structure. Together with the overall dimensions of Nsp15 (9 nm wide and 11 nm tall), this could explain why the molecules preferentially lie on their sides on the carbon support film. Since the face-on projections display 3-fold rotational
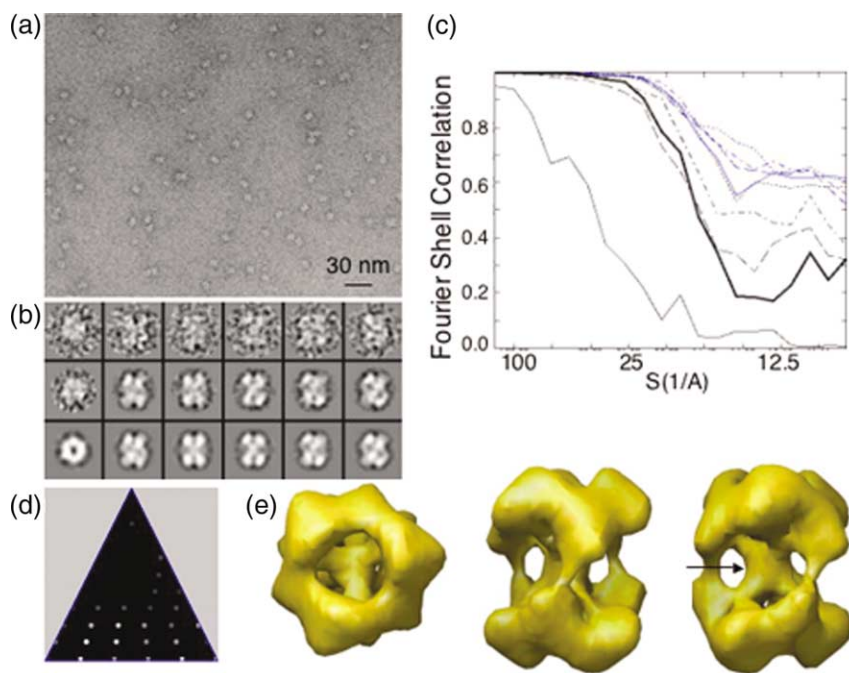
Figure 6. Single-particle analysis. (a) Electron micrograph of negatively stained Nsp15 K289A single particles. (b) Gallery of representative raw particles, class averages, and reprojections (from left to right). Boxes measure 40×40 pixels. (c) FSC plots demonstrating the progressive convergence during the refinement process. The bold line shows the resolution assessment in the final 3D reconstruction to be between 1.7 nm and 2 nm as per the 0.5 FSC criterion. (d) An asymmetric triangle depicting anisotropy with regards to the sampling of the 3D space. (e) 3D reconstruction of Nsp15K289A viewed face-on (top) and side-on (bottom). The surface rendering threshold was set to correspond to a molecular mass of 240 kDa. The arrow points at the central density.

symmetry, and that the two-layered side-on projections display 2-fold symmetry, we conclude the point group symmetry is $D3$, making Nsp15 a hexamer consisting of two trimeric rings on top of each other. These findings are in excellent agreement with the biochemical data showing that one form of Nsp15 is a hexamer.

Initial rate of catalysis as a function of protein concentration

To determine whether the enzyme was active as a hexamer, a titration experiment was performed. For accurate quantification of activity as a function of enzyme concentration, a real-time fluorescence assay was used. As previously described (K.B. *et al.*, unpublished results), this assay is based upon the substrate for ribonuclease A and consists of a tetranucleotide substrate 5′-FAM-ArUAA-3′-TAMRA, which has a 6-carboxyfluorescein linked to the 5′ end and the quencher tetramethylrhodamine at the 3′ end. Cleavage at the single riboU releases the fluorophore from the FRET quencher, allowing detection of fluorescence in real time. Nsp15, at concentrations ranging from 1 nM to 250 nM, was added to a quartz cuvette containing 1.2 μM substrate and the initial rate of cleavage was measured for 90 s. At low concentrations (1–30 nM), cleavage increased in a linear fashion relative to enzyme concentration (Figure 8). Addition of enzyme at concentrations between 30 nM and 150 nM, however, resulted in an exponential increase in rate. Addition of enzyme above 160 nM did not produce a proportionate increase in rate of cleavage, probably due to the high ratio of enzyme to substrate.

A similar analysis of the E3A mutant, which is impaired for hexamer formation, showed a similar transition in the curve, but it occurred at a higher concentration. In addition, the maximal rate of cleavage was lower for E3 than for the wild-type enzyme. Together, these results suggest that Nsp15 is enzymatically active as an oligomer, possibly a hexamer, and that oligomer formation results in cooperativity between enzyme subunits. We were unable to perform a similar analysis with E210A because the activity of this enzyme was not sufficient to obtain initial rate measurements at low enzyme concentrations. Addition of H234A at concentrations up to 300 nM to substrate revealed no significant change in fluorescence (data not shown).

Discussion

The SARS coronavirus virus encodes three proteins that are predicted to be involved in RNA processing, possibly sub-genomic RNA synthesis,[11] and therefore represent a possible target for development of antiviral drugs. One of these proteins is Nsp15, a Mn^{2+}-dependent endoribonuclease that specifically cleaves RNA at uridylate residues.[13,14] Characterizations of wild-type Nsp15 presented here demonstrate that it forms a hexamer in solution and that it is maximally active as an oligomer.

Four different approaches were used to demonstrate that Nsp15 formed hexamers. Three of these (gel-filtration, native gel electrophoresis, and ultracentrifugation) allowed the possibility to detect monomers and trimers simultaneously, when present. The patterns obtained with gel-filtration and analytical ultracentrifugation for the wild-type

(a)

(b)   (c)
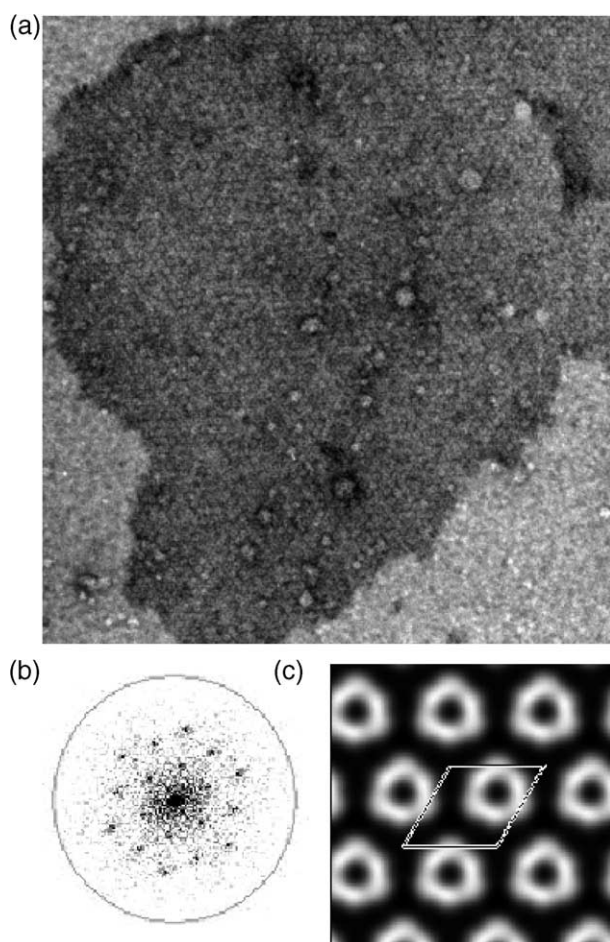
Figure 7. Two-dimensional crystallography of Nsp15. (a) Micrograph of a negatively stained 2D crystal of Nsp15K289A. (b) Fourier transform of a representative area in the crystal. The circle is drawn at a spatial frequency corresponding to 2.2 nm resolution. (c) Fourier projection map with one unit cell highlighted. ($a=b=$ 9 nm, $\gamma=120°$; *p*3).
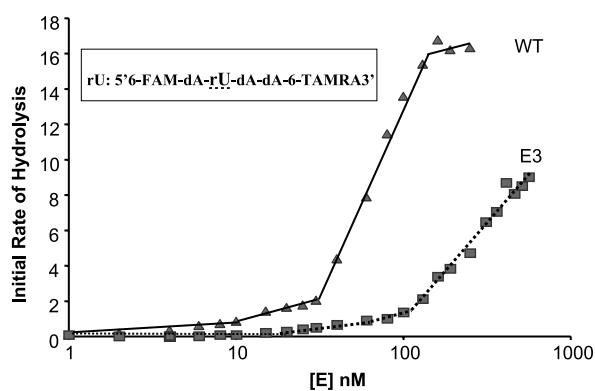
Figure 8. Initial rate of catalysis as a function of enzyme concentration. Wild-type (WT) Nsp15 or the E3A mutant were added at the indicated concentrations to 1.6 μM substrate and the increase in fluorescence was measured for 90 s. The rate of fluorescence output is plotted against concentration. The sequence of the ribonuclease substrate is shown in the box.

protein correlated well, with both indicating a ratio of approximately 85–90% hexamers at 1–5 μM Nsp15. The absence of intermediate states observed in both of these assays suggests that transition between the two forms is rapid. Gradient pore electrophoresis, however, was able to capture trimers. This is possibly due to the fact that the samples were electrophoresed until protein molecules reached a point where the polyacrylamide pore size limit their further movement. Therefore, if hexamers dissociate into trimers, their rate of migration would increase and they move into a region of the gel where the pores were too small for hexamers to reform.

The results for E3 showed the most variation among the three techniques. Gel-filtration revealed the presence of hexamers as well as monomers and trimers. This is consistent with the pore gradient electrophoresis results, as this technique yielded consistently less hexamer than the other two methods. Only hexamers and monomers were observed by ultracentrifugation, and this probably reflects the fact that normally short-lived trimers are more stable in gel-filtration than ultracentrifugation. In addition, the protein concentration in the gel-filtration experiments was fivefold higher than for ultracentrifugation. The sum of the E3 data showed that hexamer formation was impaired consistently as compared to wild-type and the other mutants under the same conditions.

Electron microscopic analysis of Nsp15 provided direct visualization of hexamers, and supported the idea of a trimeric intermediate, as the structure indicated a dimer of trimers. To our knowledge, this is the first visualization of the structure of Nsp15. There are several interesting features to note about the structure of Nsp15. (i) The protein densities that participate in the ring-like structure appear to be divided into two distinct domains, making it easy to be mistaken for a hexameric instead of a trimeric ring. One of these domains is involved in providing inter-trimeric contacts. (ii) A third domain that contributes to the pronounced central density (arrow in Figure 7(e)), may serve as a contact point for all six subunits, therefore enhancing the interactions within each trimeric ring as well as between the two trimers. (iii) Finally, the overall structure is highly cavernous, which offers many possible sites for RNA binding and processing.

The biochemical analysis presented here indicates that the hexamer structure is functionally relevant. First, the rate of RNA cleavage by Nsp15 increased exponentially with protein concentration. Second, mutation of the highly conserved N-terminal residue E3 apparently altered the subunit association constant so that the equilibrium was shifted toward monomers, which also caused a significant decrease in endoribonuclease activity. Importantly, the fact that E3 enzymatic activity was restored at higher protein concentrations argues for the higher-order structure being the enzymatically relevant one. Lastly, the mutant proteins that retained enzymatic activity also retained the ability

to form hexamers in the native gel electrophoresis assay. These results argue that the hexamer is the enzymatically active state for the SARS-CoV Nsp15 protein. The only observation inconsistent with the oligomer being the enzymatically active state is that the concentration required for enzymatic activity is lower ($\sim$0.1 μM) than the concentration needed to observe hexamer formation ($\sim$1 μM). We speculate that the difference may be due to the sensitivity of detection of the fluorescent cleavage products and the protein.

Two of the mutants with substitutions in the putative active site were affected in hexamer formation in comparison to the wild-type protein. Mutant K289A was predisposed toward hexamer formation, while the mutant H234A was less capable of forming hexamers. The high level of conservation of these residues in all coronavirus Nsp15 proteins, as well as XendoU, suggests that the affected residues are likely in the catalytic site. In fact, mutations of the residues corresponding to H234A, H249A, and K289A in XendoU decreased its endoribonuclease activity severely without an obvious effect on RNA binding.[15] Together, these results raise the possibility that catalytic activity involves recycling of hexamers from monomers or trimers, and that mutants that are unable to associate have low activity and inactive mutants do not recycle properly. Mutant H249 was apparently unaffected for hexamer formation, suggesting that not all of the putative active site residues participate in the dissociation of Nsp15 hexamers.

The finding that Nsp15 forms hexamers was unexpected. Most eukaryotic ribonucleases are either monomers or dimers. Bovine RNase A is also known to form oligomers that apparently have interesting properties. However, this is likely due to the harsh treatment of the enzyme with 50% (v/v) acetic acid.[16] One other exception is RNase PH, an exonuclease that processes the 3′ end of tRNAs.[17] This enzyme also forms a hexameric ring, but it is a trimer of dimers. Similar to our observations of the Nsp15 E3A, mutagenesis of residues essential for hexamer formation decreased the enzymatic activity of RNase PH. *E. coli* polynucleotide phosphorylase and the yeast exosome are trimeric nucleases, where each monomer contains two repeats of an RNase PH-like domain.[18,19] Hexameric rings of these molecules preclude entry of double-stranded RNA into the active site, indicating that specificity is at least partially structure-dependent.[17–19] Nsp15, which cleaves at uridylate residues, has a preference for unpaired residues (K.B. *et al.*, unpublished results), suggesting that structure may be an important determinant for substrate recognition by Nsp15.

Results from our panel of mutants correlated fairly well with previous results from Ivanov *et al.*,[13] who made a number of mutant versions in the ortholog of human coronavirus E229. They reported that substitution of alanine at sites corresponding to SARS-CoV residues H234, H249, K289, D296, and D323 resulted in inactivated enzyme. Our results in SARS-CoV confirm their results for the two histidine and the lysine mutants. We were unable to test the D296A mutant because it was insoluble. Our results with the D323A mutant contrast with the result of Ivanov *et al.*[13] because the SARS-CoV version was not severely impaired.

Currently, the role of Nsp15 in the coronavirus infection process is unknown. Several possibilities can be imagined. First, Nsp15 could be involved in SARS-CoV sub-genomic RNA synthesis. If SARS-CoV synthesizes sub-genomic RNAs by discontinuous extension of negative strands as proposed by Sawicki & Sawicki,[9] an endoribonuclease could help untether the ternary replication complex and facilitate its translocation to the leader sequence. There is precedence for such activities in viruses. An analogous nuclease activity plays a role in retrovirus replication. The RNase H activity that degrades the RNA portion of an RNA/DNA duplex releases the polymerase complex at a strong-stop sequence, after the initial round of synthesis from the tRNA primer.[20] Alternatively, if SARS uses the leader-prime mechanism for synthesis of subgenomic RNAs,[21] the nascent leader RNA could be processed by Nsp15 for use in sub-genomic synthesis. Second, Nsp15 could be involved in degradation of the minus-strand RNA. Coronavirus minus-strand RNA is highly unstable and Wang & Sawicki[22] have speculated that turnover of minus-strands regulates plus-strand RNA synthesis and decreases recognition by cellular surveillance systems that target the dsRNA intermediate. In support of this idea, it has been shown that minus-strand RNA initiates with a polyuridylate stretch,[23] a sequence that should readily be cleaved by Nsp15. Instead of, or in addition to, possible roles for Nsp15 in viral nucleic acid synthesis, Nsp15 could digest cellular RNAs, either to disrupt cellular functions or to prevent synthesis of antiviral and proapoptotic proteins. There is precedence for this in a positive-strand RNA virus. The pestiviral structural glycoprotein E^{rns} is also an endoribonuclease that can negatively affect dsRNAs that are inducers of the interferon beta response.[24] A final possibility is that Nsp15 has evolved in order to disrupt the function of the cellular homolog, EndoU, which is required for the processing of snoRNAs from their precursor RNAs.[25] The Nsp15 mutations analyzed in this study will be valuable as a guide to understanding the roles of Nsp15 *in vivo* studies. In addition, Nsp15 structural studies should benefit from the availability of mutant proteins that are defective for hexamer formation, such as E3A, and the mutants that can form hexamers, but are inactive for endoribonuclease activity.

Materials and Methods

Construction and purification of Nsp15 mutant clones

Alanine-substitution mutations in the plasmid pET15b-Nsp15[13] were constructed using the QuikChange

site-directed mutagenesis kit (Stratagene) following the protocol recommended by the manufacturer. Most of the oligonucleotides used for mutagenesis were designed to introduce silent diagnostic restriction enzyme sites, in addition to the desired alanine substitution. Potential mutant constructs were first screened by restriction enzyme digest and then the entire open reading frame was sequenced to confirm the presence of the desired mutations and the absence of additional PCR-generated errors.

His-tagged mutant and wild-type constructs were expressed in *E. coli* and purified by immobilized metal ion affinity chromatography, followed by Mono Q ion-exchange chromatography, as described.[13] The purified protein was dialyzed against 50 mM Tris (pH 7.9), 400 mM NaCl, 1 mM DTT, 50% (v/v) glycerol and stored at −20 °C. Protein concentrations were determined by SDS-PAGE analysis of serial dilutions of the Nsp15 preparations in parallel with dilutions of a bovine serum albumin (BSA) standard.

Endonuclease assays

The oligoribonucleotide SpikeTRS (CAACUAAAC-GAAC) was obtained from Dharmacon, and labeled at the 5′ end with T4 polynucleotide kinase and [γ-^{32}P]ATP. A standard RNA cleavage reaction contained 5 μM radiolabeled RNA substrate (approximately 10,000 cpm) and 25 ng (62.5 nM) of Nsp15 in a buffer of 50 mM Hepes (pH 7.2), 50 mM KCl, 1 mM dithiothreitol, 5 mM MnCl$_2$. The reaction was incubated at 30 °C for 30 min, and then terminated by the addition of a gel-loading buffer that contained 90% (v/v) formamide. Products were separated by electrophoresis in denaturing gels composed of 6 M urea and 20% (w/v) polyacrylamide on high-resolution gels or 3 M urea and 28% polyacrylamide in a mini-gel format. Gels were wrapped in plastic and exposed to a PhosphorImager screen. Each result shown was reproduced in at least two independent experiments. Quantification of radiolabeled bands was performed using a PhosphorImager (Molecular Dynamics).

Real-time assays were performed as described (K.B. *et al.*, unpublished results) using 1.2 μM fluorescent substrate (5′-FAM-ArUAA-3′-TAMRA) and protein as indicated in the same buffer that as used for the gel-based assay. The excitation wavelength was 492 nm. Changes in fluorescence at 518 nm were measured over time using an LS55 spectrometer (Perkin Elmer, Inc.).

Analytical ultracentrifugation

Sedimentation velocity experiments were performed at 4 °C with a Beckman XL-A analytical ultracentrifuge equipped with an AnTi60 rotor. Data were obtained at 30,000 rpm using a two-channel centerpiece, containing either 340 μl protein at 1 μM or buffer for reference. Absorbance data were acquired at 220 nm. Data were analyzed using the program SEDFIT and were fitted with a Lamm equation to obtain molar mass and sedimentation coefficient.[26]

Size-exclusion chromatography

Gel-filtration analyses were performed on a Pharmacia FPLC system. Protein samples (100 μg at 5 μM in 50 mM Tricine (pH 8), 300 mM NaCl, 5% glycerol, 1 mM β-mercaptoethanol) were filtered through a Superdex 200 10/30 column calibrated with the following molecular mass standards: blue dextran 2000 (2 MDa); thyroglobulin (660,000 Da); ferritin (440,000 Da); catalase (232,000 Da); aldolase (140,000 Da); BSA (67,000 Da); and chymotrypsinogen (25,000 Da) in the same buffer.

Gradient pore electrophoresis

Pore limit electrophoresis was conducted, essentially as described by Slater,[27] except that smaller and thinner gels were used and, therefore, the time needed for separation was shorter. Protein samples were loaded onto a native 4%–20% gradient gel (7 mm in length and 0.75 mm thick). Samples were electrophoresed in Tris–borate buffer (pH 8.3) for 6 h at 200 V at 4 °C, a time at which it was empirically observed that the protein ceased to migrate through the gel suggesting the different species had reached their pore exclusion. Native molecular mass markers were the same as those used for gel-filtration.

Electron microscopy

Electron microscopy used purified Nsp15 K289A mutant protein at 0.1 mg/ml in 20 mM Hepes (pH 7.0), 10 mM NaCl, 3 mM NaN$_3$. It was applied to a fresh, negatively glow-discharged, carbon-coated copper grid (G400). The molecules were allowed to absorb to the support film for 1 min at room temperature, then washed once with distilled water and negatively stained for 1 min with an aqueous solution of 1% (w/v) uranyl acetate (pH 4.25). Specimens were observed in a JEOL 1200EX transmission electron microscope operated at an acceleration voltage of 100 kV. Electron micrographs were recorded at a calibrated magnification of 39,000× on Kodak 4489 electron image sheet film. 2D crystals were obtained using essentially the same protocol but including 4% (v/v) 2-methyl-2,4-pentanediol in the buffer.

Selected electron micrographs were digitized using a Leafscan 45 microdensitometer with 5.14 Å/pixel at the specimen level. 3D reconstructions of Nsp15 K289 single particles were calculated using the EMAN software package[28] run under Linux and following procedures similar to those described by Sun *et al.*[29] Briefly, 2000 particles of Nsp15 K289 were selected using the BOXER routine, filtered, and centered. An initial 3D model was calculated from two orthogonal projections (face-on and side-on views) in *C*3 (one axis of 3-fold rotational symmetry) and subsequently refined in *D*3 (one axis of 3-fold rotational symmetry intersected by an additional orthogonal axis of 2-fold rotational symmetry). The reconstructions were iteratively refined until the structure was stable as judged by Fourier shell correlation (FSC). A molecular mass of 240 kDa was used for the surface rendering threshold of the 3D structure. 3D reconstructions were visualized using the USCF Chimera software package[30] and crystallographic images were analyzed and processed (Fourier transforms, lattice refinement, calculation of projection maps) using CRISP.[31]

were visualized using the UCSF Chimera package from the Resource for Biocomputing, Visualization, and Informatics at the University of California, San Francisco (supported by NIH P41 RR-01081).

Supplementary Data

Supplementary data associated with this article can be found, in the online version, at doi:10.1016/j.jmb.2005.09.007

References

1. Rota, P. A., Oberste, M. S., Monroe, S. S., Nix, W. A., Campagnoli, R., Icenogle, J. *et al*. (2003). Characterization of a novel coronavirus associated with severe acute respiratory syndrome. *Science*, **300**, 1394–1399.
2. Marra, M. A., Jones, S. J., Astell, C. R., Holt, R. A., Brooks-Wilson, A., Butterfield, Y. S. *et al*. (2003). The Genome sequence of the SARS-associated coronavirus. *Science*, **300**, 1399–1404.
3. Lai, M. M. C. & Cavanagh, D. (1997). The molecular biology of coronaviruses. *Advan. Virus Res.* **48**, 1–100.
4. Spaan, W., Cavanagh, D. & Horzinek, M. C. (1998). Coronaviruses: structure and genome expression. *J. Gen. Virol.* **69**, 2939–2952.
5. Gorbalenya, A. E., Snijder, E. J. & Spaan, W. J. (2004). Severe acute respiratory syndrome coronavirus phylogeny: toward consensus. *J. Virol.* **78**, 7863–7866.
6. Enserink, M. (2003). Infectious diseases. Clues to the animal origins of SARS. *Science*, **300**, 1351.
7. Pasternak, A. O., van den Born, E., Spaan, W. J. & Snijder, E. J. (2001). Sequence requirements for RNA strand transfer during nidovirus discontinuous subgenomic RNA synthesis. *EMBO J.* **20**, 7220–7228.
8. van Marle, G., Dobbe, J. C., Gultyaev, A. P., Luytjes, W., Spaan, W. J. & Snijder, E. J. (1999). Arterivirus discontinuous mRNA transcription is guided by base pairing between sense and antisense transcription-regulating sequences. *Proc. Natl Acad. Sci. USA*, **96**, 12056–12061.
9. Sawicki, S. G. & Sawicki, D. L. (1998). A new model for coronavirus transcription. *Advan. Expt. Med. Biol.* **440**, 215–219.
10. Baker, S. C. & Lai, M. M. (1990). An *in vitro* system for the leader-primed transcription of coronavirus mRNAs. *EMBO J.* **9**, 41734179.
11. Snijder, E. J., Bredenbeek, P. J., Dobbe, J. C., Thiel, V., Ziebuhr, J., Poon, L. L. *et al*. (2003). Unique and conserved features of genome and proteome of SARS-coronavirus, an early split-off from the coronavirus group 2 lineage. *J. Mol. Biol.* **331**, 991–1004.
12. Egloff, M. P., Ferron, F., Campanacci, V., Longhi, S., Rancurel, C., Dutartre, H. *et al*. (2004). The severe acute respiratory syndrome-coronavirus replicative protein nsp9 is a single-stranded RNA-binding subunit unique in the RNA virus world. *Proc. Natl Acad. Sci. USA*, **101**, 3792–3796.
13. Bhardwaj, K., Guarino, L. & Kao, C. C. (2004). The severe acute respiratory syndrome coronavirus Nsp15 protein is an endoribonuclease that prefers manganese as a cofactor. *J. Virol.* **78**, 12218–12224.
14. Ivanov, K. A., Hertzig, T., Rozanov, M., Bayer, S., Thiel, V., Gorbalenya, A. E. & Ziebuhr, J. (2004). Major genetic marker of nidoviruses encodes a replicative endoribonuclease. *Proc. Natl Acad. Sci. USA*, **101**, 12694–12699.
15. Gioia, U., Laneve, P., Dlakic, M., Arceci, M., Bozzoni, I. & Caffarelli, E. (2005). Functional characterization of XendoU, the endoribonuclease involved in small nucleolar RNA biosynthesis. *J. Biol. Chem.* **280**, 18996–19002.
16. Libonati, M. & Gotte, G. (2004). Oligomerization of bovine ribonuclease A: structural and functional features of its multimers. *Biochem. J.* **380**, 311–327.
17. Choi, J. M., Park, E. Y., Kim, J. H., Chang, S. K. & Cho, Y. (2004). Probing the functional importance of the hexameric ring structure of RNase PH. *J. Biol. Chem.* **279**, 755–764.
18. Aloy, P., Ciccarelli, F. D., Leutwein, C., Gavin, A. C., Superti-Furga, G., Bork, P. *et al*. (2002). A complex prediction: three-dimensional model of the yeast exosome. *EMBO Rep.* **3**, 628–635.
19. Symmons, M. F., Jones, G. H. & Luisi, B. F. (2000). A duplicated fold is the structural basis for polynucleotide phosphorylase catalytic activity, processivity, and regulation. *Struct. Fold. Des.* **8**, 1215–1226.
20. Peliska, J. A. & Benkovic, S. J. (1992). Mechanism of DNA strand transfer reactions catalyzed by HIV-1 reverse transcriptase. *Science*, **258**, 1112–1118.
21. Lai, M. M. C. (1990). Coronavirus: organization, replication, and expression of genome. *Annu. Rev. Microbiol.* **44**, 303–333.
22. Wang, T. & Sawicki, S. G. (2001). Mouse hepatitis virus minus-strand templates are unstable and turnover during viral replication. *Advan. Expt. Med. Biol.* **494**, 491–497.
23. Sethna, P. B., Hofmann, M. A. & Brian, D. A. (1991). Minus-strand copies of replicating coronavirus mRNAs contain antileaders. *J. Virol.* **65**, 320–325.
24. Iqbal, M., Poole, E., Goodbourn, S. & McCauley, J. W. (2004). Role for bovine viral diarrhea virus Erns glycoprotein in the control of activation of beta interferon by double-stranded RNA. *J. Virol.* **78**, 136–145.
25. Laneve, P., Altieri, F., Fiori, M. E., Scaloni, A., Bozzoni, I. & Caffarelli, E. (2003). Purification, cloning, and characterization of XendoU, a novel endoribonuclease involved in processing of intron-encoded small nucleolar RNAs in *Xenopus laevis*. *J. Biol. Chem.* **278**, 13026–13032.
26. Schuck, P. (1998). Sedimentation analysis of non-interacting and self-associating solutes using numerical solutions to the Lamm equation. *Biophys. J.* **75**, 1503–1512.
27. Slater, G. G. (1968). Pore-limit electrophoresis on a gradient of polyacrylamide gel. *Anal. Biochem.* **24**, 215–217.
28. Ludtke, S. J., Baldwin, P. R. & Chiu, W. (1999). EMAN: semiautomated software for high-resolution single-particle reconstructions. *J. Struct. Biol.* **128**, 82–97.
29. Sun, J., Savva, C. G., Deaton, J., Kaback, H. R., Svrakic, M., Young, R. & Holzenburg, A. (2005). Asymmetric binding of membrane proteins to GroEL. *Arch. Biochem. Biophys.* **434**, 352–357.
30. Pettersen, E. F., Goddard, T. D., Huang, C. C., Couch, G. S., Greenblatt, D. M., Meng, E. C. & Ferrin, T. E. (2004). UCSF Chimera–a visualization system for exploratory research and analysis. *J. Comput. Chem.* **25**, 1605–1612.

31. Hovmoller, S. (1992). CRISP–crystallographic image processing on a personal computer. *Ultramicroscopy,* **41**, 121–136.

32. Altschul, S. F., Madden, T. L., Schaffer, A. A., Zhang, J., Zhang, Z., Miller, W. & Lipman, D. J. (1997). Gapped BLAST and PSI-BLAST: a new generation of protein database search programs. *Nucl. Acids Res.* **25**, 3389–3402.

Edited by D. E. Draper